JOURNAL OF MATERIALS SCIENCE **35** (2000) 331–335

Texture instability in Ni electrodeposits applied in optical disk technology

F. CZERWINSKI*, J. A. SZPUNAR
Department of Metallurgical Engineering, McGill University, Montreal, Que., Canada
E-mail: frankcz@minmet.lan.mcgill.ca

An x-ray diffraction technique was used to assess the thermal transformation of the crystallographic texture in 300 μm thick Ni electrodeposits applied in optical disks technology. The initially strong ⟨100⟩ fiber texture was transformed during annealing to ⟨211⟩ fiber and the temperature range for rapid changes was between 300 and 350 °C. A numerical analysis of texture data indicates that the grain boundaries with a low and high misorientation angle ($<30^\circ$ and $>45^\circ$) had mobility advantage and their migration contributed to the growth of the ⟨211⟩ texture. © *2000 Kluwer Academic Publishers*

1. Introduction

Optical recording devices were first developed in 1965 and today, all personal computers come with CD-ROM drives, and almost everyone who listens to music owns a CD player and CD's [1]. The major attraction of optical disk systems is a very high data storage capacity, virtually instant access to the desired data, fidelity and low cost [2]. The reason a single disk can hold such a great amount of data is because of the tightly focused laser beams used to create the pits in the disks.

The manufacturing process of optical recording disks involves their replication from metal templates called stampers using a high injection molding press. The stampers are produced by electrodeposition of Ni on the substrate containing the recording pattern, which was created by the laser lithography. The structure of the electrolytic metal is, however, thermodynamically unstable and prone to change at the elevated temperatures of the replication [3, 4]. Since structural changes deteriorate the stamper hardness and wear resistance, which increases the error rate of disks manufactured, their assessment is of engineering importance.

Recent studies of the thermal stability of electrodeposits are concerned mainly with nanocrystalline materials in order to preserve their special properties at higher temperatures. Nanocrystalline Ni with an initial grain size between 10 and 30 nm, showed abnormal grain growth at temperatures above 200 °C and the activation energy ranged from 1.2 to 1.4 eV [5]. There is no agreement in the literature on how to explain the thermal evolution of the microstructure in Ni electrodeposits. While some studies attribute the changes to grain growth rather than recrystallization [6, 7], other supports the presence of all stages typical for recovery, recrystallization and abnormal grain growth [8]. Our preliminary tests revealed that the crystallographic texture seems to be very sensitive to temperature increase. Texture studies may, therefore, help to understand and improve the structural stability of the electrodeposits at elevated temperatures.

This paper contains an x-ray analysis of the texture transformation in Ni electrodeposits at elevated temperatures. The texture data are used to assess the changes of grain boundary character distribution.

2. Experimental

The Ni stampers in the form of disks with a diameter of over 130 mm and a thickness of 0.3 mm, electrolytically deposited from a Watt's bath by Saturn Solutions Inc., were used as research material in this study. Deposition was conducted at a temperature of 50 °C and at a current density of 1 A/dm^2. Annealing was performed in a flowing argon atmosphere at temperatures ranging from 300 up to 800 °C for 0.5 h. The textures of Ni after deposition and annealing were measured using a D-500 Siemens x-ray goniometer and Mo K_α radiation. Pole figures data were collected using the reflection technique up to a maximum tilt of 80° in 5° polar and radial intervals. The results were corrected for absorption and defocusing based on the standard random specimen, prepared from Ni powder. The experimental pole figures were then used to calculate the orientation distribution functions (ODF) of the grains by applying the procedure described by Bunge [9]. The morphological characterization involved atomic force microscopy (AFM), Digital Instruments Nanoscope III. Microhardness was tested using a LECO M-400 instrument with a Vickers indentor under a load of 200 g.

3. Results

3.1. Morphology and texture of as-deposited Ni

The surface morphology of the electrodeposit, created by the molding of the laser lithography pattern of the

* On leave from the University of Mining and Metallurgy, Krakow, Poland.

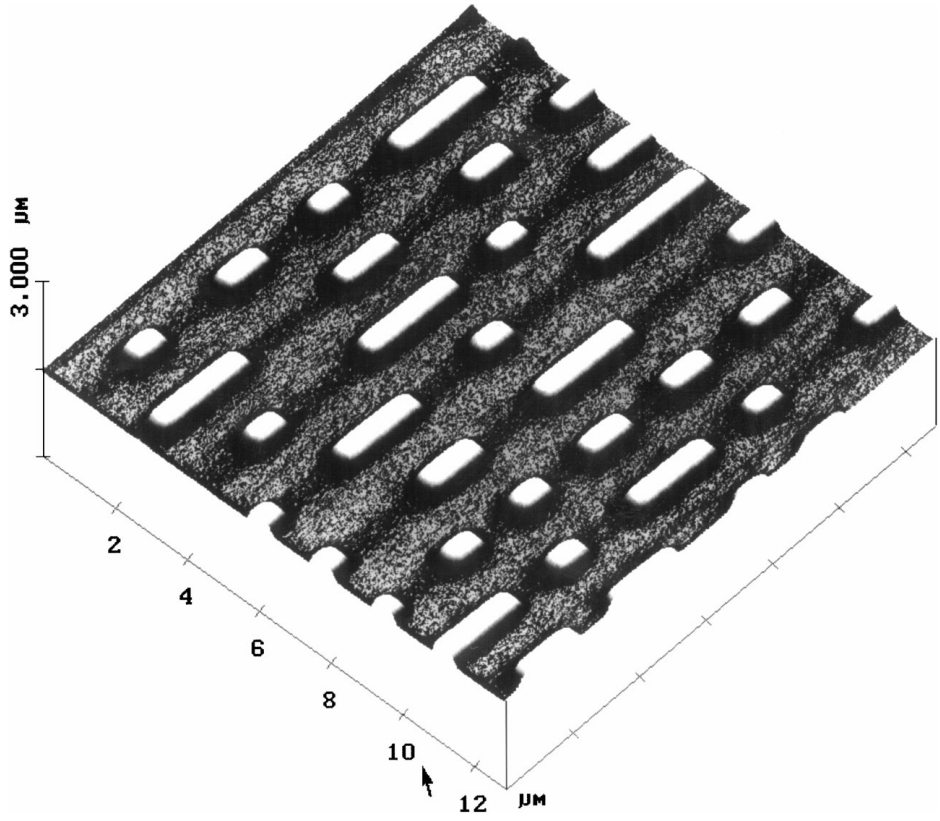

Figure 1 AFM image of the Ni electrodeposit surface containing the recording pattern.

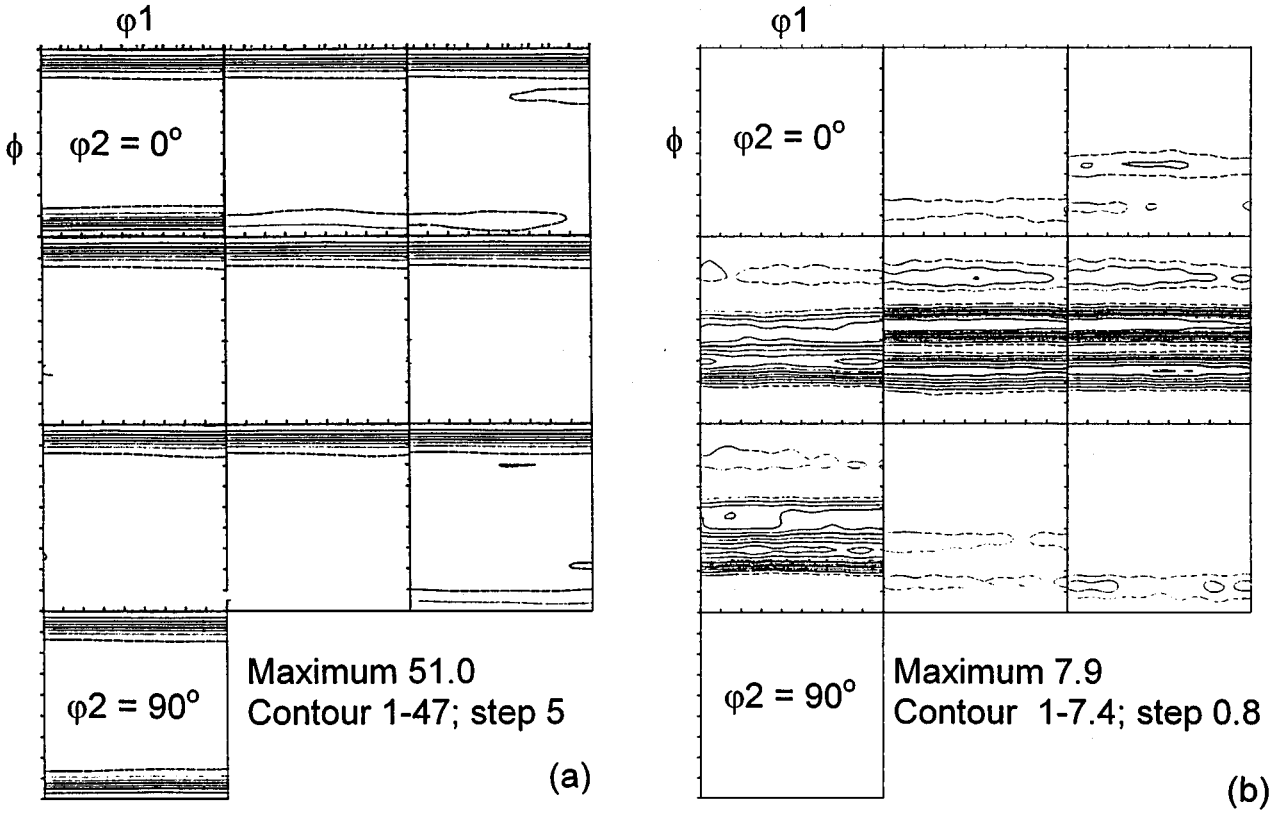

Figure 2 Orientation distribution functions (ODF) of Ni grains after deposition (a) and after annealing at 600 °C for 0.5 h (b). The standard coordinates (φ_1, ϕ, φ_2) are used in φ_2 projection according to Bunge's formalism [9].

substrate, is shown in Fig. 1. The essential features of this topography, which contains encoded information, are the regular bumps with a width of approximately 300 nm and various heights, generally between 150 and 200 nm.

In the as-deposited state, the orientation of Ni grains was represented by the ⟨100⟩ fibre texture, with the {100} planes aligned parallel to the deposit surface. This texture is represented by the ODF in Fig. 2a. According to notation by Bunge [9], the standard coordinates (φ_1,

ϕ, φ_2) are applied in φ_2 projection. There was some texture inhomogeneity across the deposit thickness. The major change was an increase in pole density from 61.5 on the outer surface to 64.1 at a depth of approximately 10 μm beneath it. Here, we confined our investigations to the vicinity of the outer surface, adjacent to the bumps. The ⟨100⟩ texture is essentially expected for Watt's bath and the current density in the range between 1 and 10 A/dm^2. According to the diagram by Froment and Maurin [10], the ⟨100⟩ texture should be surrounded by the ⟨110⟩ texture region for a current density below 1A/dm^2 and by the area of ⟨210⟩ and ⟨110⟩ textures for current densities larger than 10 A/dm^2. A lack of texture components other than the ⟨100⟩ suggests that the current densities during deposition did not exceed the above ranges.

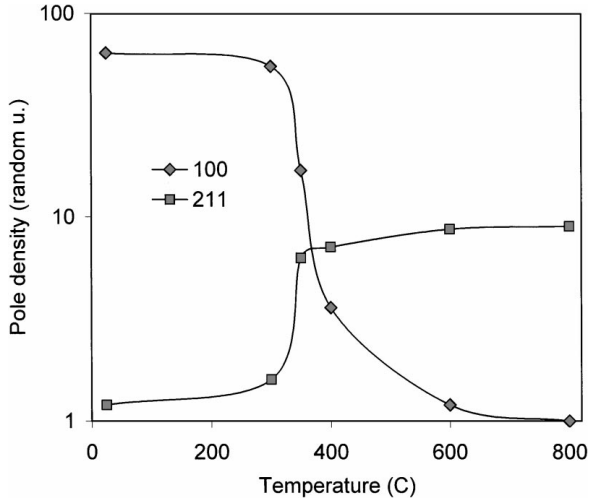

Figure 3 The semi-logarithmic plot of the texture evolution in Ni electrodeposit as a function of annealing temperature. Annealing time of 0.5 h.

3.2. Texture transformation during annealing

An example of the deposit texture after annealing is shown in Fig. 2b. While the ⟨100⟩ component disappeared, the ⟨211⟩ fibre dominated the deposit texture in the annealed state. The evolution of the Ni texture as a function of the annealing temperature is shown in Fig. 3. The intensity for ⟨211⟩ texture was taken from the centre of the {211} pole figures, which were recalculated from orientation distribution functions. It is seen that critical changes in the texture took place between 300 and 350 °C. The range of the rapid texture changes coincides with a sharp reduction in the deposit hardness from above 200 to 85 HV.

3.3. Structure of Ni grain boundaries

In order to understand the mechanism of texture transformation, changes in the geometry of the grain boundaries were assessed. Various representations are developed to describe grain boundary statistics in polycrystalline materials [11, 12]. A grain boundary can be classified geometrically in terms of the relative misorientation between the adjacent grains (GBMD), calculated from experimental ODF data. The calculation was carried out by finding out the misorientation between an assumed orientation and a randomly created orientation in accordance with the measured ODF [13]. The changes of GBMD during annealing are shown in Fig. 4a in the form of histograms plotted for four ranges of misorientation angles between grains. In general, low and high misorientations represent the grain boundaries with low energy. The histograms show that annealing leads to a reduction in the percentage of grain boundaries with misorientation below 30°. The fractions of grain boundaries with that misorientation in both as-deposited and annealed Ni is still higher than

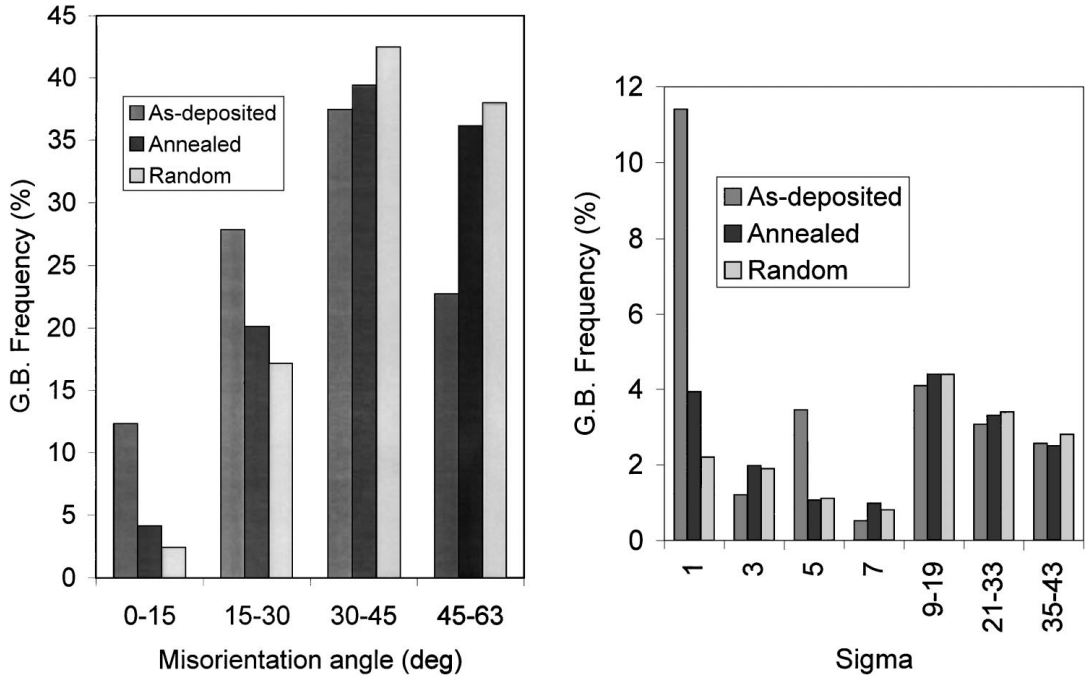

Figure 4 The grain boundary characteristics in Ni as-deposited and annealed for 0.5 h at 600 °C: (a) misorientation angle between grains; (b) selected types of special grain boundaries. Values marked as random are the frequencies expected for material without texture.

that expected in material without texture. The annealing led to an increase in the fractions of grain boundaries with misorientations above 45°. For this angle range, the fractions of grain boundaries either in as-deposited or annealed materials were still lower than values calculated for the random orientation of grains.

In order to complete the grain boundary misorientation analysis, special grain boundaries were identified. Special grain boundaries are described by the parameter Σ, which is the reciprocal density of common sites in the coincidence site lattice (CSL) model [14]. A boundary is usually classified as belonging to a certain Σ value if the deviation from an exact CSL is specified by Brandon criteria [15]. It is known that the frequency of the occurrence of CSL boundaries in polycrystalline materials is affected by texture, correlation between orientations of neighbouring grains, inhomogeneities and grain size.

The computer program used in this study allows for the investigation of the relationship between the presence of special misorientations and texture under the assumption of the absence of a spatial correlation between grain orientations [13]. The calculations of CSL and GBMD were carried out for 100,000 grains to minimize the statistical error. The resultant CSL histograms are shown in Fig. 4b, where grain boundaries are divided into several categories: $\Sigma 1$, $\Sigma 3$, $\Sigma 5$, $\Sigma 7$, $\Sigma 9$–19, $\Sigma 21$–33 and $\Sigma 35$–43. For the purpose of comparison, the CSL distribution, which is expected for a specimen prepared from a powder, with randomly oriented grains, is also included. The results show that after deposition the total contribution of special grain boundaries with $\Sigma 1$–43 is about 26%, which is significantly higher than values reported for textured metallurgical materials [13]. Excluding $\Sigma 1$–5, the other CSL boundaries have fractions below 1%. The only significant change observed after annealing is a reduction in the percentage of $\Sigma 1$ and $\Sigma 5$ boundaries.

4. Discussion of results

These experiments show that the microcrystalline electrodeposits are prone to thermal changes, in quite a similar way as that revealed for nanocrystalline structures [16]. It is also clear that crystallographic texture is a very sensitive indicator of structural evolution. The ⟨100⟩ texture in as-deposited Ni is typical for Watt's electrolyte and the intermediate values of current densities [10]. The initial texture is extremely strong and with intensities exceeding the level of 60 random units is over one order of magnitude stronger than textures reported previously for nanocrystalline Ni and Ni-based electrodeposits [17, 18]. There is a general belief that the ⟨100⟩ texture in Ni and Ni-based alloys is unstable at elevated temperatures. The most common texture after annealing is the ⟨111⟩ fibre.

There is no single factor, which totally controls the texture transformation. The initial texture is one of them. Our previous research showed that the coarse grain Ni with an initial texture of ⟨110⟩ transformed after annealing to ⟨210⟩ and ⟨100⟩ changed to the ⟨111⟩. At the same time the ⟨211⟩ was replaced by a mixture of the ⟨111⟩ + ⟨100⟩ [19]. In Ni with a nanometer size grains the double texture of ⟨111⟩ + ⟨100⟩ transformed to the weak ⟨111⟩ fibre [18]. However, when the same nanocrystalline Ni was heated up rapidly, it developed the ⟨311⟩ fibre instead of the ⟨111⟩. The above examples indicate the complexity of texture transformation.

At present, there is no general explanation of texture evolution during the annealing of electrodeposits. The model proposed recently for copper [20] assumes that the recrystallized grains orient themselves so that the minimum elastic modulus direction can be parallel to the maximum normal stress direction of the original grains. Since the minimum elastic modulus directions of copper are the ⟨100⟩, the ⟨100⟩ of the original grains, being the directions of the Burgers vectors, tend to be oriented along the ⟨100⟩ directions of the recrystallized grains. Unfortunately, his mechanism cannot be directly adopted for Ni because in Cu the opposite phenomenon is observed. After annealing, the ⟨100⟩ texture is the most stable component, developed in deposits with initial textures of ⟨100⟩ or ⟨111⟩ [20].

Since there is some analogy between electrodeposited and cold deformed metallurgical materials, one should consider mechanisms proposed to explain texture development during the recrystallization of steels. The major theory of the {110}⟨001⟩ (Goss) texture formation in conventional grain-oriented electrical steel assumes that grains with {110}⟨001⟩ orientation form colonies and, as a result of coalescence during annealing, develop size-advantage [21]. Another theory assumes that the {110}⟨001⟩ grains are surrounded by the highest number of CSL boundaries, which are supposed to have high migration mobility [22]. A recent explanation states that {110}⟨001⟩ grains are surrounded by the highest number of high-energy grain boundaries [23]. These grain boundaries have a high migration rate due to the fast coarsening of the precipitates. The results of the numerical analysis of texture data in this study indicate the changes in grain boundary character distribution after annealing. It is clear that the growing ⟨211⟩ texture has 15% less in the frequency of grain boundaries with a misorientation angle below 30° and 15% more grain boundaries with a misorientation angle above 45°. It is known, however, that these boundaries have lower energy when compared to boundaries with intermediate misorientations.

The explanation of the high mobility of low energy boundaries in electrolytic Ni can be proposed while considering its specific microstructure. It consists of a mixture of micrometer-size grains and ultra-fine grains with a size in the order of a hundred nanometers [24]. The ultra-fine grains in the electrodeposits are attributed to the higher stored strain energy [25]. Since non equilibrium grain boundary structure results in high mobility, the grain growth starts in their regions. While considering the nano-size grains, the energy of their grain boundaries differs from conventional microcrystalline materials. In particular, the grain boundaries in nanocrystals are highly disordered and their energy is less anisotropic than that known in microcrystalline counterparts [26, 27]. This energy is marked as E_n in Fig. 5. A lack of its dependence on a misorientation

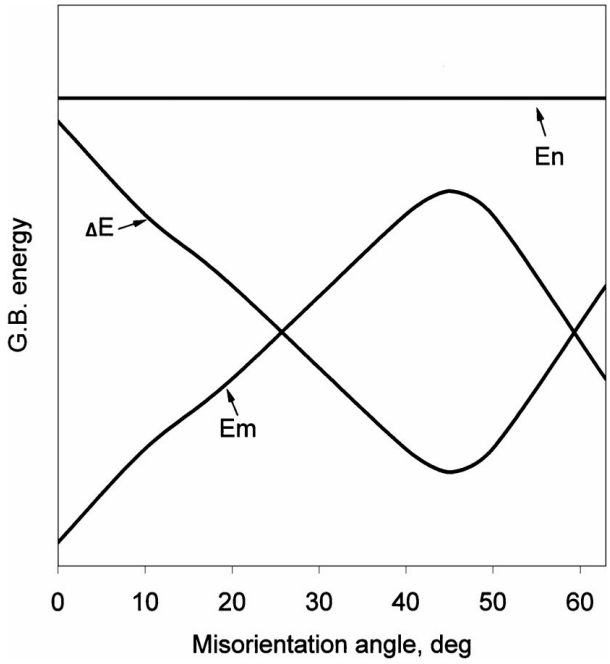

Figure 5 The schematic diagram of the energy of grain boundaries in nano and microcrystalline materials as a function of misorientation angle.

angle is caused by the fact that energy is stored in short segments of grain boundaries and in the dense network of the grain boundary junctions. The energy of grain boundaries in conventional polycrystalline material, marked as E_m in Fig. 5, clearly depends on the grain misorientation angle [11, 12]. Assuming the difference in grain boundary energy before and after annealing, $\Delta E = E_n - E_m$, is a driving force for grain boundary migration, it can be concluded that the grain boundaries with low and high misorientations have a mobility advantage. This may explain why these boundaries control the transformation of the texture during the annealing of the Ni electrodeposit.

5. Conclusions

As-deposited structures of electrolytic Ni, applied for stampers in the replication of CD-ROM disks, exhibit an extremely strong ⟨100⟩ fibre texture with an axis perpendicular to the deposit surface. The ⟨100⟩ texture is thermally unstable and transforms at elevated temperatures to the significantly weaker ⟨211⟩ fibre. The temperature range of rapid texture changes is between 350 and 400 °C, and corresponds to the sharp decrease in deposit hardness.

The texture transformation leads to changes in Ni grain boundary character distribution. Based on the numerical analysis of texture data, the reduction in the number of grain boundaries with a misorientation angle below 30° is accompanied by an increase in the number of grain boundaries with a misorientation above 45°. Of all the special grain boundaries with Σ below 43, there is mainly a reduction in the fraction of Σ1 and Σ5.

Acknowledgement

The authors thank the Saturn Solutions Inc., Montreal, Canada, for providing the specimens for investigation.

References

1. J. WROBEL, *Solid State Technol.* **32**(6) (1989) 103.
2. R. LESSOR, *Defense Electronics* **9** (1993) 27.
3. F. CZERWINSKI, *J. Mater. Sci.* **33** (1998) 3831.
4. A. W. THOMPSON and H. J. SAXTON, *Metall. Trans.* **4** (1973) 1599.
5. I. KAUR, W. GAUST and L. KOZMA (eds.), "Handbook of Grain and Interface Boundary Diffusion Data," Vol. 2 (Ziegler Press, Stuttgart, 1989) p. 1037.
6. E. J. SUONINEN and T. HAKKARAINEN, *J. Mater. Sci.* **3** (1968) 446.
7. R. WEIL, H. J. SUMKA and G. W. GREENE, *J. Electrochem. Soc.* **114** (1967) 449.
8. B. E. JACOBSON and J. W. SLIWA, *Plating and Surface Finishing* **9** (1979) 42.
9. H. J. BUNGE, "Texture Analysis in Materials Science" (Butterworth, London, 1982).
10. M. FROMENT and G. MAURIN, *J. Microscopie* **7** (1968) 37.
11. T. WATANABE, *Mater. Sci. Forum* **46** (1989) 25.
12. A. P. SUTTON and R. W. BALLUFFI, "Interfaces in Crystalline Materials" (Clarendon, Oxford 1995).
13. A. MORAWIEC, J. A. SZPUNAR and D. C. HINZ, *Acta Metall. Mater.* **41** (1993) 2825.
14. H. GRIMMER, M. BOLLMANN and D. H. WARRINGTON, *Acta Crystallogr.* **30** (1974) 197.
15. D. G. BRANDON, *Acta Metall.* **14** (1966) 1479.
16. U. KLEMENT, U. ERB, A. M. SHERIK and K. T. AUST, *Mater. Sci. Eng.* **A203** (1995) 177.
17. F. CZERWINSKI, H. LI, F. MEGRET, J. A. SZPUNAR, D. G. CLARK and U. ERB, *Scripta Mater.* **37** (1997) 1967.
18. F. CZERWINSKI, G. PALUMBO and J. A. SZPUNAR, *ibid.* **39** (1998) 1359.
19. F. CZERWINSKI and J. A. SZPUNAR, *Corrosion Sci.* **41** (1999) 729.
20. D. N. LEE, *Mater. Res. Proc.* **427** (1996) 167.
21. M. MATSUO, *ISIJ International* **29** (1989) 809.
22. J. HARASE, R. SHIMIZU and D. J. DINGLEY, *Acta Metall.* **39** (1991) 763.
23. Y. HAYAKAWA and J. A. SZPUNAR, *Acta Mater.* **45** (1997) 1285.
24. F. CZERWINSKI and J. A. SZPUNAR, *ibid.* **47** (1999) 2553.
25. F. CZERWINSKI, *J. Electroch. Soc.* **143** (1996) 3327.
26. S. R. PHILLIPOT, D. WOLF and H. GLEITER, *J. Appl. Physics* **78** (1995) 847.
27. *Idem., Scripta Metall. Mater.* **33** (1995) 1245.

Received 9 December 1998
and accepted 12 July 1999